Draft version August 4, 2025
Typeset using LaTeX **twocolumn** style in AASTeX7



# A Novel Formation Channel for Supermassive Black Hole Binaries in the Early Universe via Primordial Black Holes

Saiyang Zhang [1,2] Boyuan Liu [3,4] and Volker Bromm [2,5]

[1] Department of Physics, University of Texas at Austin, Austin, TX 78712, USA
[2] Weinberg Institute for Theoretical Physics, Texas Center for Cosmology and Astroparticle Physics, University of Texas at Austin, Austin, TX 78712, USA
[3] Institute of Astronomy, University of Cambridge, Madingley Road, Cambridge, CB3 0HA, UK
[4] Universität Heidelberg, Zentrum fur Astronomie, Institut für Theoretische Astrophysik, D-69120 Heidelberg, Germany
[5] Department of Astronomy, University of Texas at Austin, Austin, TX 78712, USA

## ABSTRACT

We present a novel formation channel for supermassive black hole (SMBH) binaries in the early Universe, driven by primordial black holes (PBHs). Using high-resolution hydrodynamical simulations, we explore the role of massive PBHs ($m_{\rm BH} \sim 10^6\ M_\odot$) in catalyzing the formation of direct-collapse black holes (DCBHs), providing a natural *in situ* pathway for binary SMBH formation. PBHs enhance local overdensities, accelerate structure formation, and exert thermal feedback on the surrounding medium via accretion. Lyman-Werner (LW) radiation from accreting PBHs suppresses $H_2$ cooling, shifting the dominant gas coolant to atomic hydrogen. When combined with significant baryon–dark matter streaming velocities ($v_{\rm b\chi} \gtrsim 0.8\ \sigma_{\rm b\chi}$, where $\sigma_{\rm b\chi}$ is the root-mean-square streaming velocity), these effects facilitate the formation of dense, gravitationally unstable atomically-cooling gas clouds in the PBH's wake. These clouds exhibit sustained high inflow rates ($\dot{M}_{\rm infall} \gtrsim 0.1 - 0.01\ M_\odot\,{\rm yr}^{-1}$), providing ideal conditions for DCBH formation from rapidly growing supermassive stars of $\sim 10^5\ M_\odot$ at redshift $z \sim 20-10$. The resulting systems form SMBH binaries with initial mass ratios $q \sim \mathcal{O}(0.1)$ and separations of $\sim 10$ pc. Such PBH-DCBH binaries provide testable predictions for JWST and ALMA, potentially explaining select high-$z$ sources like Little Red Dots (LRDs), and represent gravitational wave sources for future missions like LISA and TianQin—bridging early-Universe black hole physics, multi-messenger astronomy, and dark matter theory.

*Keywords:* Dark matter (353) — Early universe (435) — Galaxy formation (595) — Population III stars (1285) — Supermassive black holes (1663)

## 1. INTRODUCTION

The unprecedented capabilities of the James Webb Space Telescope (JWST) have revolutionized our understanding of the early Universe, unveiling a substantial population of supermassive black holes (SMBHs) at high redshifts of $z \gtrsim 7$ (e.g., A. D. Goulding et al. 2023; R. L. Larson et al. 2023; Á. Bogdán et al. 2024; J. E. Greene et al. 2024; O. E. Kovács et al. 2024; R. Maiolino et al. 2024; P. Natarajan et al. 2024; L. Napolitano et al. 2024; R. Maiolino et al. 2025). Among the most intriguing findings from JWST are "Little Red Dots" (LRDs), compact sources identified at $4 < z < 9$, whose nature remains enigmatic (e.g., I. Labbé et al. 2023; I. Labbe et al. 2025; V. Kokorev et al. 2024; D. D. Kocevski et al. 2024; G. C. K. Leung et al. 2024; A. J. Taylor et al. 2024). Concurrently, JWST observations also report instances of galaxy mergers at high redshift $z \gtrsim 6$ (H. Übler et al. 2024; Y. Matsuoka et al. 2024), highlighting dynamic environments capable of hosting SMBH binaries even in the early Universe. Recently, binary SMBHs have been proposed to explain the unusual spectral characteristics of LRDs (K. Inayoshi et al. 2025), suggesting a direct observational link between high- and lower-redshift binary black hole populations.

Conventionally, within the ΛCDM cosmological framework, SMBH binaries are understood to originate from both *in situ* and *ex situ* channels. The *in situ* channel involves the fragmentation of the pristine gas cloud into massive star clusters, and merging stellar remnants

Email: szhangphys@utexas.edu, boyuan.liu@uni-heidelberg.de

will eventually form binary massive BHs (e.g., S. Hirano et al. 2018; M. A. Latif et al. 2020; T. E. Woods et al. 2024). On the other hand, the *ex situ* channel involves hierarchical galaxy mergers (e.g., S. D. M. White & M. J. Rees 1978; S. D. M. White & C. S. Frenk 1991), as a standard scenario for massive galaxy growth. If each merging galaxy harbors a central SMBH that is massive enough ($\gtrsim 10^8\ M_\odot$, L. Ma et al. 2021), dynamical friction efficiently removes angular momentum, causing black holes to migrate toward the galaxy center and form gravitationally bound binary systems on parsec-scale separations (e.g., M. C. Begelman et al. 1980; L. Valtaoja et al. 1989; M. Milosavljević & D. Merritt 2003a,b).

Those SMBH binaries are proposed to contribute significantly to the gravitational wave background (GWB) signals (G. Hobbs & S. Dai 2017; J. D. Romano & N. J. Cornish 2017), detectable by current Pulsar Timing Arrays (PTAs) at nanohertz frequencies (e.g., A. Sesana 2013; G. Agazie et al. 2023; H. Xu et al. 2023; D. J. Reardon et al. 2023; EPTA Collaboration et al. 2023). Detecting and characterizing these signals will provide crucial insights into the SMBH formation mechanisms, evolution pathways, and merger rates throughout cosmic time. Furthermore, these SMBH binaries can serve as powerful electromagnetic wave emitters, observable across multiple wavelengths from optical to X-rays (e.g., C. Roedig et al. 2014; L. Č. Popović 2012; J. R. Westernacher-Schneider et al. 2022), enriching our understanding of their environments, accretion processes, and host galaxy properties in the local Universe.

Motivated by both observational and theoretical developments, we propose a novel formation channel for SMBH binaries via the direct-collapse mechanism induced by primordial black holes (PBHs). Direct-collapse black holes (DCBHs) represent astrophysically-seeded black holes, emerging in the early Universe, under peculiar conditions for violent gravitational collapse of metal-poor gas clouds (A. Loeb & F. A. Rasio 1994; V. Bromm & A. Loeb 2003; M. C. Begelman et al. 2006; G. Lodato & P. Natarajan 2006; C. Reisswig et al. 2013; M. Suazo et al. 2019; M. A. Latif et al. 2020; S. Chon & K. Omukai 2020). On the other hand, PBHs constitute one of the well-motivated dark matter candidates (for a general review, see B. Carr & F. Kühnel 2020), theorized to form shortly after the Big Bang via the collapse of overdense regions (Y. B. Zel'dovich & I. D. Novikov 1967; S. Hawking 1971; B. J. Carr 1975; K. M. Belotsky et al. 2019; A. Escrivà 2022). Previous investigations have explored the impact of PBHs on cosmic thermal history (e.g., M. Ricotti et al. 2008; Y. Ali-Haïmoud & M. Kamionkowski 2017; V. De Luca et al. 2020; P. Lu et al. 2021; F. Ziparo et al. 2022; S. Zhang et al. 2024b; C. Casanueva-Villarreal et al. 2025), structure formation (e.g., P. Meszaros 1975; N. Afshordi et al. 2003; A. Kashlinsky 2021; N. Cappelluti et al. 2022; B. Liu & V. Bromm 2023; S. Zhang et al. 2024a), and the seeding of early galaxies and SMBHs (e.g., K. J. Mack et al. 2007; B. Carr & J. Silk 2018; D. Inman & Y. Ali-Haïmoud 2019; B. Liu et al. 2022; B. Liu & V. Bromm 2022; Y. Lu et al. 2024; H.-L. Huang et al. 2024; P. E. Colazo et al. 2024; F. Ziparo et al. 2024; S. Zhang et al. 2025; P. Dayal & R. Maiolino 2025; L. R. Prole et al. 2025). These studies underscore the rich astrophysical phenomena arising within PBH models, intensively examined through both simulations and analytical frameworks.

Here, we simulate the evolution of the structure around an isolated massive PBH ($\sim 10^6\ M_\odot$) and study the critical conditions for potential secondary black hole formation. This particular PBH mass scale is motivated by the change in the equation of state during the $e^+e^-$ annihilation epoch within cosmic thermal history, when the temperature of the universe is $T \sim 1$ MeV (B. Carr et al. 2021). Specifically, we explore how the presence of soft-UV, Lyman-Werner (LW) radiation from BH accretion flows interacts with $H_2$ and $H^-$ within the gas cloud through photo-dissociation (B. T. Draine & F. Bertoldi 1996; T. Abel et al. 1997), thus suppressing their abundance and consequently reducing the gas cooling efficiency. Therefore, different from S. Zhang et al. (2025), under this LW radiation, we focus mainly on the fate of the pristine gas cloud surrounding the PBH and find the condition for runaway collapse of this cloud into a DCBH. For the cases where secondary black holes form, we make predictions for the evolution of such binary systems and discuss the possible implications for future observations of their electromagnetic and gravitational wave signals.

In Section 2, we describe the numerical recipes for our simulations in detail, including the black hole accretion feedback model and criterion for collapsing gas cloud formation. Following the simulation, we analyze the formation of dense cores and the inflow of gas and discuss the criterion for DCBH formation in Section 3. The potential implications on binary black hole formation and possible observational signatures are discussed in Section 4, followed by conclusions drawn in Section 5.

In our simulations, we adopt *Planck18* cosmological parameters throughout ( Planck Collaboration et al. 2020): $\Omega_{\rm m} = 0.3111$, $\Omega_{\rm b} = 0.04897$, $h = 0.6776$, $\sigma_8 = 0.8102$, $n_{\rm s} = 0.9665$.

**Table 1.** Summary of key parameters and main results. $L$ is the size of the box in comoving units. $z_{\rm ini}$ is the initial redshift where the simulation starts, and $z_{\rm col}$ the redshift when collapsing sink particles begin to aggregate around the central PBH [a]. $N_{\rm eff}$ is the total number of particles within the simulation box. $\epsilon_r$ is the thermal feedback coupling efficiency. $m_{\rm col}$ denotes the total mass of the collapsing cloud that formed in the PBH-hosting halo by the end of the simulation ($z \sim 10$). STR is a flag indicating whether the relative streaming of PDM and gas particles is included (✓) or not (✗), and the value represents the amplitude with respect to the root-mean-square streaming velocity $\sigma_{\rm bX}$. BH_LW is another flag to control whether we include (✓) the local LW feedback from BH accretion or not (✗).

| Run | $L$ [ckpc] | $z_{\rm ini}$ | $z_{\rm col}$ | $N_{\rm eff}$ | $\epsilon_{\rm r}$ | $m_{\rm col}[M_\odot]$ | STR | BH_LW |
|---|---|---|---|---|---|---|---|---|
| CDM*[b] | 250 | 1100 | - | $2\times256^3$ | - | - | ✗ | - |
| PBH_fd005* | 250 | 1100 | - | $2\times256^3$ | 0.005 | - | ✗ | ✗ |
| PDMonly* | 250 | 3400 | - | $256^3$ | - | - | - | - |
| PBH_LW_fd05 | 250 | 1100 | - | $2\times256^3$ | 0.05 | - | ✗ | ✓ |
| PBH_LW_fd005 | 250 | 1100 | - | $2\times256^3$ | 0.005 | - | ✗ | ✓ |
| PBH_LW_fd0005 | 250 | 1100 | - | $2\times256^3$ | 0.0005 | - | ✗ | ✓ |
| PBH_LW_wstr_fd005 | 250 | 1100 | - | $2\times256^3$ | 0.005 | - | 0.4 ✓ | ✓ |
| PBH_LW_str_fd005 | 250 | 1100 | 17.41 | $2\times256^3$ | 0.005 | $5.23\times10^4$ | 0.8 ✓ | ✓ |
| PBH_LW_mstr_fd005 | 250 | 1100 | 11.71 | $2\times256^3$ | 0.005 | $5.33\times10^4$ | 1.2 ✓ | ✓ |
| PBH_LW_sstr_fd005 | 250 | 1100 | 14.96 | $2\times256^3$ | 0.005 | $9.76\times10^4$ | 1.6 ✓ | ✓ |

[a]Different from S. Zhang et al. (2025), limited by computational resources, we terminate the simulations at about $z \gtrsim 10$ when the timestep becomes extremely small or when star formation takes place in halos faraway from the PBH.
[b]The simulation runs denoted with * are taken from S. Zhang et al. (2025).

## 2. METHODOLOGY

We explore the evolution of gas dynamics around an isolated PBH at high redshift, using the state-of-the-art simulation package GIZMO (P. F. Hopkins 2015). In Section 2.1, we first describe the simulation code and the initial condition settings. Different from previous work, we focus on the LW photons emitted from BH accretion flows with an improved intensity fitting model (V. Takhistov et al. 2022; B. Liu et al. 2022). We then describe the BH accretion model (V. Springel 2005; M. Tremmel et al. 2017), and the implementation of our updated feedback prescription in Section 2.2. Last, in Section 2.3, we discuss the criterion for the identification of collapsing gas particles as part of a dense gas core (i.e., the potential formation site of a DCBH). For convenience, Table 1 summarizes the relevant initial conditions and parameters used in our simulations.

### 2.1. *Simulation and Initial Conditions*

We implement our simulations with the GIZMO code (P. F. Hopkins 2015), employing the Lagrangian meshless finite-mass (MFM) solver for hydrodynamics combined with a comprehensive primordial chemistry network (see, V. Bromm et al. 2002; J. L. Johnson & V. Bromm 2006; B. Liu & V. Bromm 2018), and the parallelized Tree+PM gravity solver for N-body dynamics from GADGET-3 (V. Springel 2005).

We simulate the initial growth of structure around a PBH with a particle dark matter (PDM)-only pathfinder run denoted as `PDMonly`, from the beginning of the matter dominated era at $z_{\rm eq} = 3400$ to the recombination epoch ($z = 1100$), using the initial conditions generated with the MUSIC code (O. Hahn & T. Abel 2011), placing an isolated PBH at the center of the box [6]. The mass of the PBH is denoted by $m_{\rm BH}$, setting it to be $10^6\ M_\odot$ throughout. The simulation box has a side length of $L \sim 250$ ckpc, with a total of $N_{\rm PDM} = 256^3$ particles to resolve the PDM component[7]. Using the Zel'dovich approximation (Y. B. Zel'dovich 1970) and the numerical recipes from previous work (Y. Ali-Haïmoud & M. Kamionkowski 2017; D. Inman & Y. Ali-Haïmoud 2019; B. Liu & V. Bromm 2023; S. Zhang et al. 2024a), the displacement and velocity perturbations of PDM particles induced by the PBH are calculated and added in the initial box. Different from S. Zhang et al. (2024a), we have improved the calculation of linear and non-linear perturbation growth by adapting the numerical recipe from H. Jiao et al. (2024). The growth factor of linear perturbations is rescaled to reproduce the long-term growth of halos seeded by isolated PBHs from the spherical collapse theory (K. J. Mack et al. 2007).

[6] Our PBH initial condition generator PHANTOM is publicly available on GitHub: https://github.com/Sylvanzsy/pbh_cosmosim_ics

[7] As discussed in S. Zhang et al. 2025, our simulations represent an effective PBH mass fraction of less than $6\times10^{-4}$, set by the ratio of the PBH mass to the total mass enclosed within the simulation volume. This limit is consistent with existing constraints and agrees with previous simulation results, exploring varying PBH density fractions.

At $z = 1100$, when baryons and photons start to decouple, we include an additional uniform baryon matter field with the same resolution as PDM in the initial condition set up, resulting in a total number of $N = 2\times256^3$ particles with a mass of $\sim 100(18)\ M_\odot$ for PDM (gas) particles. With this setting, we both approximate the initial structure of PDM around the PBH, and let the gas collapse onto this PBH-seeded halo. In running these simulations, the softening length of PDM and gas is set to $\epsilon_{\rm PDM} = \epsilon_{\rm gas} \sim 0.01\, L/N_{\rm PDM}^{1/3} \simeq 0.01\ h^{-1}$kpc, and the initial chemical abundances are assigned to the values predicted for the intergalactic medium (IGM) at $z = 1100$, as summarized in D. Galli & F. Palla (2013).

In addition, we also consider the relative streaming motion between gas and PDM particles by assigning a universal velocity offset. In our earlier work (S. Zhang et al. 2025), we found that streaming can enhance, rather than delay, galaxy formation—contrary to the conclusion generally reached within the standard ΛCDM framework (e.g., A. T. P. Schauer et al. 2019, 2023). This enhancement arises from a displacement in the center of mass (away from the PBH) caused by the relative motion between baryons and dark matter, leading to star formation in the dense gas structures that form in the wake of the PBH. These wake-driven overdensities promote gravitational collapse and thus play a catalytic role in early star formation. To systematically explore the impact of streaming velocity on black hole formation, we implement a velocity offset parameterized as a multiple of the root-mean-square streaming velocity $\sigma_{\rm b\chi} = 30\ {\rm km\,s^{-1}}$. Specifically, we consider four cases with velocity offsets of 0.4, 0.8, 1.2, and 1.6 $\sigma_{\rm b\chi}$, corresponding to simulation runs labeled as `PBH_LW_wstr_fd005`, `PBH_LW_str_fd005`, `PBH_LW_mstr_fd005` and `PBH_LW_sstr_fd005`, respectively.

### 2.2. *Black Hole Accretion and Feedback*

In the early Universe where the cosmic density field is nearly uniform and isotropic, we use a Bondi-Hoyle formalism to approximate the BH accretion rate, as

$$\begin{aligned}\dot{m}_{\rm acc} &= \frac{4\pi(Gm_{\rm BH})^2\rho_{\rm gas}}{\tilde{v}^3} = \frac{4\pi(Gm_{\rm BH})^2\rho_{\rm gas}}{(c_s^2+v_{\rm gas}^2)^{3/2}} \\ &\simeq 0.0072\ M_\odot{\rm yr}^{-1}\left(\frac{10\ {\rm km/s}}{\tilde{v}}\right)^3 \\ &\times\left(\frac{n_{\rm H}}{1\ {\rm cm^{-3}}}\right)\left(\frac{m_{\rm BH}}{10^6\ M_\odot}\right)^2, \end{aligned} \tag{1}$$

where $\rho_{\rm gas} = \mu m_{\rm H} n_{\rm H}$ is the average density of the gas sampled from the BH accretion kernel, and $\mu = 1.22$ is the average molecular weight. Here, $c_s$ and $v_{\rm gas}$ are the sound speed and velocity dispersion of the surrounding gas, averaged over the gas particles within the accretion kernel. The size of the BH accretion kernel, defined as the region that determines the BH accretion rate, is set to the Bondi radius calculated from the last timestep $r_{\rm Bondi} \sim 2Gm_{\rm BH}/c_s^2$.

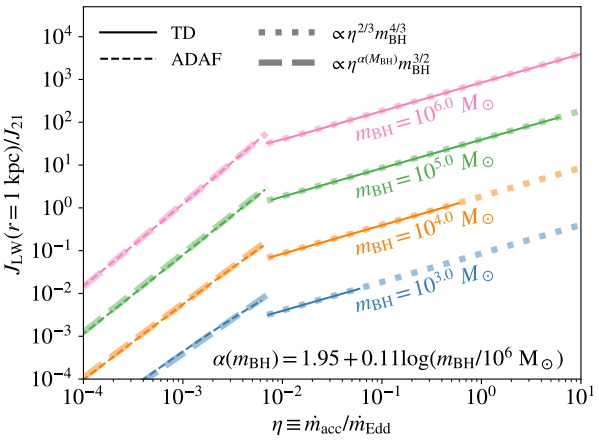


**Figure 1.** Normalized Lyman–Werner (LW) intensity, $J_{\rm LW}/J_{21}$, as a function of the Eddington ratio, $\eta \equiv \dot{m}_{\rm acc}/\dot{m}_{\rm Edd}$, for black holes of varying masses ($m_{\rm BH} = 10^3, 10^4, 10^5, 10^6\ M_\odot$). The $J_{\rm LW}$ values are computed at a distance of $r = 1$ kpc from the black hole. The results based on the semi-analytical spectra models for TD and ADAF accretion profiles in V. Takhistov et al. (2022) are shown by the thin solid and dashed lines, respectively. Here, the ADAF regime is only expected to occur at low accretion rates ($\eta \lesssim 0.007$), best fitted with $J_{\rm LW} \propto \eta^{\alpha(m_{\rm BH})} m_{\rm BH}^{3/2}$, where $\alpha(m_{\rm BH}) = 1.95 + 0.11\log\left(m_{\rm BH}/10^6\ {\rm M}_\odot\right)$ (Eq. 4; thick dashed lines). The TD regime, occurring at higher accretion rates ($\eta > 0.007$), satisfies the scaling relation $J_{\rm LW} \propto \eta^{2/3} m_{\rm BH}^{4/3}$ (Eq. 4; thick dotted lines).

From the calculated accretion rate, we update the BH mass at each timestep $\delta t$ by $\delta m_{\rm BH} = \dot{m}_{\rm acc}\delta t$. To ensure mass and momentum conservation, we adopt the algorithm from V. Springel (2005), in which the BH particle stochastically swallows nearby gas particles to remain consistent with the average growth rate, and a drag force is applied according to the momentum of the swallowed gas.

During the accretion process, the feedback energy is injected into the surrounding gas particles by a volume-weighted average, following the prescription in V. Springel (2005). At the end of each timestep $\delta t$, the total amount of energy injected is $\delta E = \epsilon_r \epsilon_{\rm EM} \dot{m}_{\rm acc} c^2 \delta t$. Here, $\epsilon_r$ is the thermal coupling coefficient and we take it as a free parameter to study its variational effect at high redshift. $\epsilon_{\rm EM}$ is the radiative efficiency parameter, calculated according to the subgrid model in A. Negri

& M. Volonteri (2017), as

$$\epsilon_{\rm EM} = \frac{\epsilon_0 A\eta}{1+A\eta}\ , A = 100\ , \tag{2}$$

capturing the transition from the geometrically thick, radiatively inefficient advection-dominated accretion flow (ADAF) regime to a radiatively efficient thin-disk (TD) one. Here $\eta$ is the Eddington ratio defined by $\eta \equiv \dot{m}_{\rm acc}/\dot{m}_{\rm Edd}$, where the Eddington accretion rate $\dot{m}_{\rm Edd}$ is given by

$$\dot{m}_{\rm Edd} = 0.047\ M_\odot\ {\rm yr}^{-1} \left(\frac{\rm m_{BH}}{10^6\ {\rm M}_\odot}\right)\left(\frac{\epsilon_0}{0.057}\right)^{-1}, \tag{3}$$

adopting $\epsilon_0 = 0.057$ as the radiative efficiency in the thin-disk accretion model for non-spinning BHs considering that PBHs are born with very low spins ($\lesssim 0.01$) in the canonical scenario of Gaussian perturbations (e.g., V. De Luca et al. 2019; M. Mirbabayi et al. 2020).

To estimate the LW radiation intensity, we use fitting formulae in the form of a broken power-law model to capture both the TD and the ADAF regimes, as illustrated in Figure 1. Here, the ADAF regime is only expected to occur at low accretion rates ($\eta \lesssim 0.007$), transitioning to the TD regime at higher rates. The specific LW intensities are obtained by integrating the spectra modeled in V. Takhistov et al. (2022) within the photon energy range $h\nu \sim 11.2$–$13.6$ eV. We can write the intensity (in units of $J_{21} = 10^{-21}$ erg s$^{-1}$ cm$^{-2}$ sr$^{-1}$ Hz$^{-1}$) at a distance $r$ from an accreting BH as a function of BH mass $m_{\rm BH}$ and Eddington ratio $\eta$ (see Fig. 1):

$$\frac{J_{\rm LW}}{J_{21}} \simeq \begin{cases} 9\times10^5 \eta^{1.95+0.11\log\left(m_{\rm BH}/10^6\ {\rm M}_\odot\right)} \\ \left(\frac{m_{\rm BH}}{10^6\ {\rm M}_\odot}\right)^{3/2}\left(\frac{r}{\rm kpc}\right)^{-2} & \text{(ADAF)}, \\ 8.8\times10^2\eta^{2/3} \\ \left(\frac{m_{\rm BH}}{10^6\ {\rm M}_\odot}\right)^{4/3}\left(\frac{r}{\rm kpc}\right)^{-2} & \text{(TD)}. \end{cases} \tag{4}$$

Once $J_{\rm LW}$ is known, we combine it with the local gas shielding factor (J. Wolcott-Green et al. 2011) to derive the dissociation rates of $H^-$ and $H_2$ following S. Zhang et al. (2025, see their sec. 2.2).

### 2.3. *Gravitational Instability*

In previous work (S. Zhang et al. 2025), we found that under the effect of LW radiation from BH accretion, a dense gas clump with mass $\mathcal{O}(10^5)M_\odot$ was identified in the vicinity of the PBH, evolving along the atomic hydrogen cooling track (S. P. Oh & Z. Haiman 2002). Therefore, to further assess whether this gas clump will collapse and may eventually lead to the formation of a DCBH, we here impose an explicit density threshold criterion, $n_{\rm H} \gtrsim 10^6$ cm$^{-3}$, for the formation of collapsing clouds. This value is close to the maximum density resolved within our simulations. It is also chosen to be larger than the density threshold for cloud collapse ($n_{\rm H} \gtrsim 10^4$ cm$^{-3}$) found in previous work, as the "Zone of no return" (K. Inayoshi et al. 2014).

To determine whether a gas particle can partake in the collapse or is engulfed by the central BH, we first calculate the local free-fall time of the gas:

$$t_{\rm ff} = \sqrt{\frac{3\pi}{32G\rho_{\rm gas}}} \simeq 0.47\ {\rm Myr}\left(\frac{10^4\ {\rm cm}^{-3}}{n_{\rm H}}\right)^{1/2}, \tag{5}$$

using the local gas density $\rho_{\rm gas}$. We calculate this timescale once the critical density threshold is reached and compare it to the time, $t_{\rm survive}$, that the particle survives without being accreted by the PBH.

If this collapsing particle survives the accretion and is not reheated by black hole thermal feedback, such that it can reach $t_{\rm survive} \gtrsim t_{\rm ff}$, we convert it into a sink particle as part of the collapsing gas cloud. However, once the gas particle fails to meet the density collapse criterion while still registering $t_{\rm survive} \lesssim t_{\rm ff}$, we reset the timer to $t_{\rm survive} = 0$ in the following time step, and will not start the timer unless it again satisfies the density threshold criterion. We have also established by numerical experimentation that, during the initial collapse at $z \gtrsim 200$, gas densities could reach as high as $n_{\rm H} \gtrsim 10^6$ cm$^{-3}$ in the vicinity of the PBH, thus formally satisfying the collapse criterion mentioned above[8]. However, subsequent shock waves generated during the accretion will rapidly terminate this efficient accretion phase, smoothing out any dense structures around the PBH that have not been accreted. Therefore, to avoid numerical artifacts, we prohibit the formation of collapsing particles as an additional constraint at $z \gtrsim 200$.

To facilitate our analysis, we introduce $N_{\rm col}$ as the cumulative number of sink particles and start to output snapshots when $N_{\rm col} = 1$. Whenever $N_{\rm col}$ doubles, a simulation snapshot is generated to record the detailed time evolution of this dense atomically-cooling gas cloud. Note that the sink particles do not represent individual stars but are only meant to estimate the mass

[8] The initial collapse is induced by the PBH seeding effect, where gas is attracted by the potential well forming overdense regions (for a similar effect without PBHs, see e.g., S. Hirano et al. 2015; M. Ito & K. Omukai 2024; W. Qin et al. 2025). During this process, the imbalance between the thermal pressure from BH feedback and the gravitational pressure from the gas cloud results in gas collapsing onto the PBH and formation of dense regions near the PBH, greatly boosting the accretion efficiency (see fig. 2 in S. Zhang et al. 2025).

of collapsing gas that would form stars and DCBHs at the limit of our resolution. The detailed star and DCBH formation processes unresolved here are deferred to further work.

## 3. RESULTS AND DISCUSSION

In exploring our key results, we first identify the formation of a dense gas core within our simulation box in Section 3.1. By tracking the inflow of gas towards this dense core, we identify the criterion for the potential gas collapse and subsequent DCBH formation in Section 3.2.

### 3.1. *Dense Core Formation*

In the standard DCBH scenario (e.g., V. Bromm & A. Loeb 2003; M. C. Begelman et al. 2006; G. Lodato & P. Natarajan 2006), the collapse of massive pristine gas clouds (metallicity $Z \lesssim 10^{-4} Z_\odot$) occurs under rare conditions that involve strong LW radiation from neighboring galaxies. Under these conditions, the gas gravitationally collapses without significant fragmentation and proto-stellar feedback into an initial protostar at the center (F. Becerra et al. 2018a,b), rapidly accreting the surrounding gas to form a supermassive star (SMS). This SMS subsequently undergoes instability-triggered collapse into a massive black hole seed of mass $\sim 10^5\ M_\odot$ at redshift $z \sim 10-15$ (e.g., M. Shibata & S. L. Shapiro 2002; T. Hosokawa et al. 2013; C. Reisswig et al. 2013; L. Haemmerlé et al. 2018; L. Haemmerlé 2021; C. Nagele et al. 2022; N. P. Herrington et al. 2023; M. Shibata et al. 2025).

In this study, we introduce a crucial modification to this canonical scenario by incorporating accretion feedback from a central PBH as the LW radiation source, rather than relying on neighboring galaxies. The LW radiation generated by PBH accretion suppresses the abundance of molecular hydrogen ($H_2$) in the surrounding gas, significantly altering its cooling efficiency. Building on our previous work (S. Zhang et al. 2025), we demonstrate that massive PBHs enhance local overdensities, expediting the formation of DM halos and attracting the surrounding gas from the IGM, while simultaneously introducing thermal feedback that delays gas cooling and collapse. In this study, we focus on conditions for DCBH formation around a fiducial heating efficiency value of $\epsilon_r \sim 0.5\%$, previously identified by S. Zhang et al. (2025) as critical to the formation of collapsing gas clouds in the absence of LW radiation.

Another vital condition explored in our study is the baryon-DM relative streaming velocity (e.g., A. Stacy et al. 2011; A. T. P. Schauer et al. 2017, 2019). Unlike the standard ΛCDM scenario, where streaming velocities typically delay the formation of collapsing gas clouds, our simulations suggest that streaming effects can enhance collapse by creating dense pockets of gas behind the PBH trajectory through the IGM. This effect becomes particularly significant at higher initial streaming velocities ($v_{b\chi} \gtrsim 0.8\sigma_{b\chi}$), emphasizing the critical role of streaming velocities in promoting the formation of massive pristine gas clouds. Conversely, as demonstrated in our `PBH_LW_wstr_fd005` and `PBH_LW_fd005` runs, lowering the initial streaming velocity reduces the offset between the PBH and the gas cloud's center of mass, causing dense gas during the initial collapse phase to be rapidly engulfed by the central black hole.

An illustrative example of the gas collapse process is presented in Figure 2, capturing the onset of collapse from the `PBH_LW_str_fd005` simulation at $z \simeq 17.4$. Similar to S. Zhang et al. (2025), cold gas flows in from the IGM at speeds of $\sim 50\ \mathrm{km\,s^{-1}}$, competing against the hot gas outflows due to BH accretion and forming a dense gas cocoon around the PBH. The collapse occurs within a dense pocket, characterized by a compact core radius of $\lesssim \mathcal{O}(1)\,\mathrm{pc}$. At $\sim$10 pc from the PBH, the collapsing gas cloud reaches a hydrogen number density of $n_\mathrm{H} \sim 10^6\ \mathrm{cm^{-3}}$ and a temperature of $T \sim 10^4$ K, while the central PBH accretes at roughly 1% of its Eddington rate. Using these parameters in Equ. (4), we calculate a LW radiation intensity of $J_\mathrm{LW}/J_{21} \sim 4 \times 10^5$, which greatly exceeds the critical threshold of $J_\mathrm{crit} \sim 10 - 10^3$ necessary for $H_2$ suppression (e.g., K. Sugimura et al. 2014; B. Agarwal et al. 2016; A. Trinca et al. 2022), implying dominant atomic hydrogen cooling[9]. A similar gas configuration is also observed in the `PBH_LW_sstr_fd005` run at $z \sim 15$ and in the `PBH_LW_mstr_fd005` run at $z \sim 11.7$, with collapsing particles similarly positioned relative to the PBH. Although variations in initial relative streaming velocities were tested, no clear correlation emerged between streaming velocity amplitudes and collapse initiation times. This implies a stochastic nature of DCBH formation around PBHs, and future studies should consider multiple random realizations for each streaming velocity to evaluate the statistics and possible trends.

Figure 3 provides further details on the conditions necessary for gas cloud collapse under LW radiation through phase diagrams depicting temperature ($T$) versus hydrogen number density ($n_\mathrm{H}$) when the first collapsing particles were identified. These diagrams display sev-

[9] The physics behind this critical value is rather complex (e.g., T. E. Woods et al. 2019), so instead we show a range of values here from the literature.

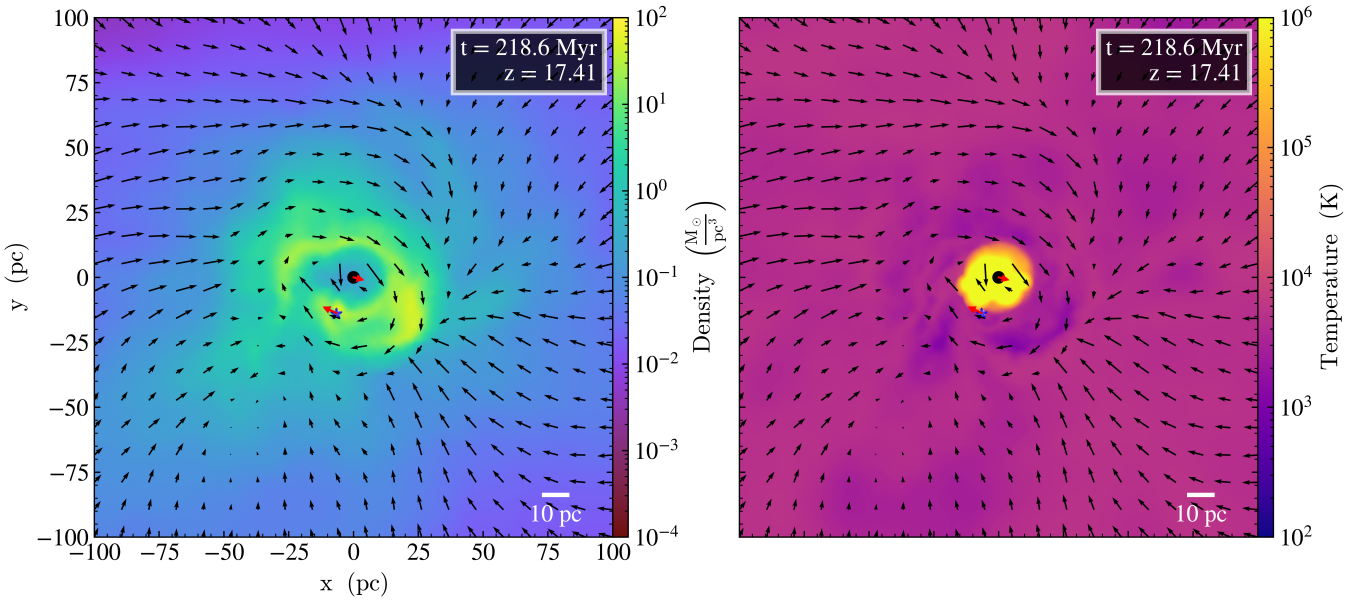


**Figure 2.** Onset of gaseous cloud collapse. We show projections of gas density (**left panel**) and temperature (**right panel**) for the gas surrounding the central PBH taken from the `PBH_LW_str_fd005` simulation, within a physical 200 pc scale. The snapshot is taken at $z \simeq 17.4$, corresponding to the moment where the first collapsing sink particle emerges. The simulation assumes a BH thermal feedback efficiency of $\epsilon_r = 0.5\%$, a relative streaming velocity of $v_{b\chi} = 0.8\ \sigma_{b\chi}$, and includes the LW radiation generated during PBH accretion. The black dot marks the position of the PBH, while the blue star indicates the location of the collapsing gas cloud, representing the site for potential DCBH formation. Red arrows denote the relative motions between the central PBH and bulk velocity of the collapsing gas cloud. Velocity vectors for gas are overlaid on both panels, with arrow sizes scaled by magnitude (different from that for BHs) to illustrate the inflow of gas toward the PBH, as well as feedback-driven outflows in its vicinity.

eral simulation settings[10]: the baseline `CDM` simulation at $z = 14.9$, the `PBH_fd005` run without LW radiation at $z = 29.6$, the `PBH_LW_fd005` run at $z = 10.6$, and the `PBH_LW_str_fd005` run at $z = 17.4$. A constant feedback efficiency of $\epsilon_r = 0.5\%$ is assumed for simulations containing a PBH. These phase diagrams illustrate substantial variations in cooling pathways, especially a shift from molecular hydrogen cooling (in the `CDM` and `PBH_fd005` runs) to atomic cooling (in the `PBH_LW_fd005` and `PBH_LW_str_fd005` runs) under LW radiation. The bifurcation in the `PBH_LW_fd005` case is reflecting the collapse of pristine gas through $H_2$ cooling within halos $\sim$15 kpc away from the central PBH where $J_{\rm LW} < J_{\rm crit}$, such that the thermal evolution there is not significantly affected by LW radiation. In this case, moreover, the gas surrounding the PBH is cooling via atomic hydrogen, thus exhibiting a nearly isothermal trend. However, this gas cloud is never able to reach densities of $n_{\rm H} \gtrsim 10^4$ cm$^{-3}$ before being accreted or evaporated by the BH, thus avoiding runaway collapse until the end of the simulation. Notably, the `PBH_LW_str_fd005` simulation highlights the key role of (sufficiently strong) baryon-DM streaming in triggering the collapse of dense, quasi-isothermal gas clouds ($\sim 10^5\ M_\odot$, $T \sim 8000 - 9000$ K, and $n_{\rm H} \gtrsim 10^4$ cm$^{-3}$).

[10] Note that the results for the `CDM` and `PBH_fd005` runs are reproduced from S. Zhang et al. (2025), where LW radiation backgrounds were absent and the collapse of gas was governed by a Jeans instability criterion.

### 3.2. *Mass Inflow and DCBH Formation Criterion*

To further elucidate the evolution of the collapsing gas cloud and the conditions conducive to DCBH formation, we closely analyze the temporal progression of the infall rate and mass accumulation within the collapsing region. As demonstrated in Figure 4, simulation cases including the effect of streaming with $v_{b\chi} \gtrsim 0.8\sigma_{b\chi}$ (`PBH_LW_sstr_fd005`, `PBH_LW_mstr_fd005` and `PBH_LW_str_fd005`) result in the formation of massive collapsing clouds $\sim$6 Myr after the initial collapse. Throughout this process, the gas infall rate consistently exceeds $\gtrsim 10^{-3}\ M_\odot\,{\rm yr}^{-1}$, with peak values frequently surpassing $\gtrsim 10^{-2}\ M_\odot\,{\rm yr}^{-1}$. In our simulations, since accretion onto sink particles was not implemented and the resolution limit does not extend to the length scale of a proto-star, we approximate the gas infall rate onto the proto-star by differentiating the total collapsing particle masses with respect to time.

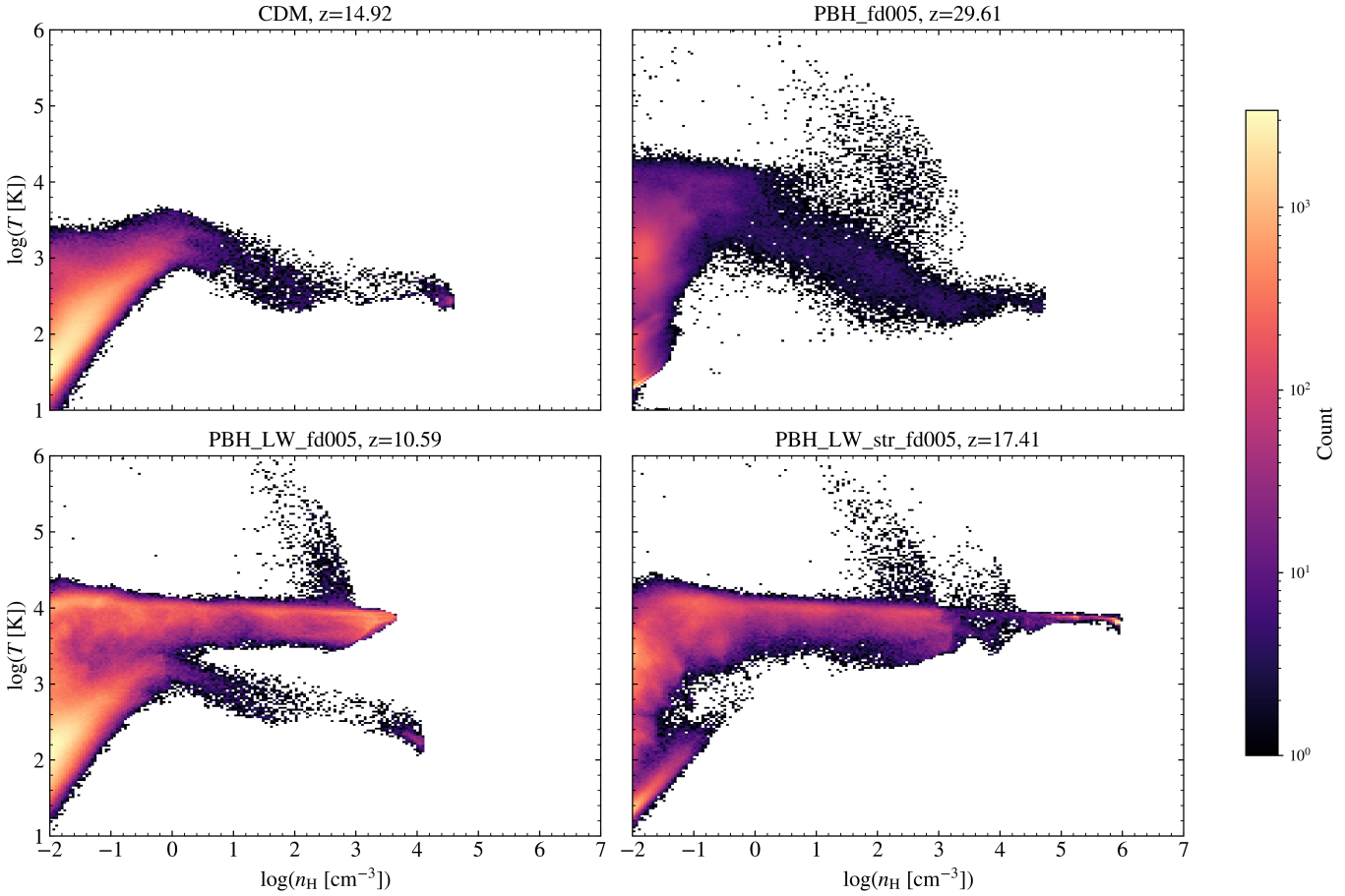


**Figure 3.** Gas properties in the vicinity of the central PBH. We present phase diagrams of temperature ($T$) vs. hydrogen number density ($n_{\rm H}$) for several simulation runs at the moment where collapsing particles were first identified. The simulation without a PBH (`CDM`) and without Lyman–Werner (LW) feedback from BH accretion (`PBH_fd005`) are included as a reference (taken from S. Zhang et al. 2025) to demonstrate the effects of PBH accretion heating and LW feedback on the surrounding gas. For the runs with PBHs (`PBH_fd005`,`PBH_LW_fd005` and `PBH_LW_str_fd005`), the same feedback efficiency of $\epsilon_r = 0.005$ is assumed. The effect of including LW radiation is demonstrated in the lower panels with the `PBH_LW_fd005` (left) and `PBH_LW_str_fd005` (right) runs, showcasing the change in the thermal evolution of the gas. The additional effect in the presence of baryon–DM streaming is evident in the `PBH_LW_str_fd005` run, where successful runaway collapse along the near-isothermal atomic cooling track is triggered.

To interpret these inflow rates physically, we compare them with characteristic values associated with both Pop III star formation and DCBH formation (see also B. Liu et al. 2024). In zeroth order, the gas infall rate for a self-gravitating spherical gas cloud can be estimated by dividing the Jeans mass by the free-fall timescale (e.g., S. W. Stahler et al. 1980):

$$\dot{M}_{\rm infall} \sim \frac{M_{\rm J}}{t_{\rm ff}} \simeq \frac{c_s^3}{G} \simeq 4 \times 10^{-3} \left(\frac{T_{\rm gas}}{10^3\ {\rm K}}\right)^{3/2} M_\odot\,{\rm yr}^{-1}. \quad (6)$$

For gas cooled predominantly via atomic hydrogen with temperatures of $T_{\rm gas} \sim 5000 - 10^4$ K, the gas inflow rates naturally exceed the critical rate required for DCBH formation via (feedback-free, bloated) SMSs $\sim 0.01 - 0.1\ M_\odot\,{\rm yr}^{-1}$ (see e.g., L. Haemmerlé et al. 2018; K. Inayoshi et al. 2020; N. P. Herrington et al. 2023; B. Liu et al. 2024). Conversely, gas clouds undergoing molecular cooling typically exhibit temperatures of $\sim 400 - 1000$ K, corresponding to a typical inflow rate of $\sim 10^{-2} - 10^{-3}\ M_\odot\,{\rm yr}^{-1}$ for conventional Pop III star formation scenarios (e.g., V. Bromm 2013; R. S. Klessen & S. C. O. Glover 2023). Our simulated results show mass inflow rates frequently exceeding the critical threshold for DCBH formation, consistent with the simulations of SMS growth in atomic cooling clouds in the standard ΛCDM model (e.g., D. Toyouchi et al. 2023).

Further examination of the compact core formed in our simulations reveals rapid mass growth to approximately $5 \times 10^4 - 10^5\ M_\odot$ within $\sim 6$ Myr, consistent with

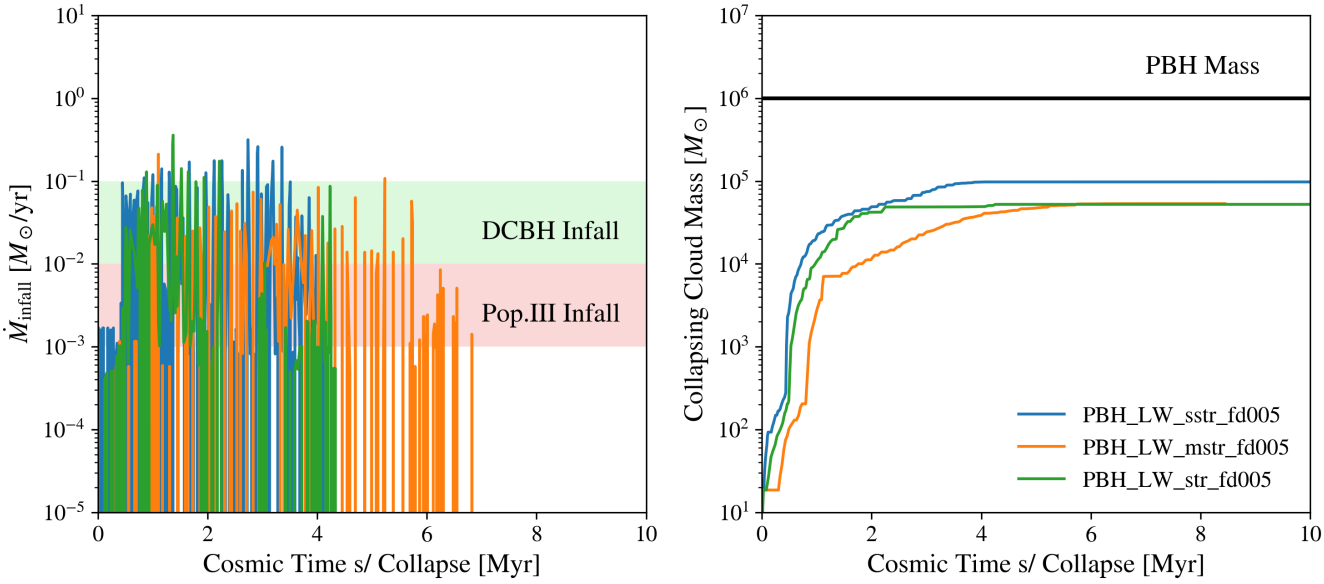


**Figure 4.** Evolution of gas infall rate (**left panel**) and total collapsing cloud mass (**right panel**) as a function of cosmic time since the initial collapse event, comparing select simulation scenarios: `PBH_LW_sstr_fd005` (blue), `PBH_LW_mstr_fd005` (orange) and `PBH_LW_str_fd005` (green). The left panel compares our simulation results with typical inflow rates encountered in Pop III star formation ($\sim 10^{-2} - 10^{-3}\ M_\odot\,{\rm yr}^{-1}$; light-red shading) and the critical rate required for DCBH formation ($\sim 0.01 - 0.1\ M_\odot\,{\rm yr}^{-1}$; light-green shading). The right panel summarizes the growth of the collapsing cloud mass within $\sim 5$ Myr of cosmic time, approaching values characteristic of DCBH seeds ($\sim 10^5\ M_\odot$), comparing to the primary PBH mass ($\sim 10^6\ M_\odot$; solid line). As can be seen, cases that combine LW feedback with the presence of (strong) baryon-DM streaming encounter conditions favorable for massive black hole seed formation.

theoretical expectations for DCBH seed masses (e.g., F. Becerra et al. 2018a; M. A. Latif et al. 2022; S. Chon & K. Omukai 2025). The sustained elevated inflow rate thus strongly supports rapid mass accumulation onto the core, indicating a clear pathway for the formation of a supermassive object in the center of the cloud. Additionally, comparing the mass of the central PBH to the mass of the newly formed collapsed core, we find a mass ratio of approximately $q \sim 0.05 - 0.1$, confirming the formation of a massive binary system.

## 4. EMPIRICAL SIGNATURES

The SMBH binary formation scenario explored in this study has significant implications for current and future observational efforts across both the electromagnetic (EM) and gravitational wave (GW) domains, providing a promising pathway for multi-messenger astrophysics (see e.g., A. De Rosa et al. 2019). Detecting such signals would enhance our understanding of SMBH binary formation mechanisms, accretion processes, and mass evolution, directly linking theoretical predictions from early-Universe scenarios to observable gravitational wave phenomena.

SMBH binaries originating from this PBH-induced DCBH pathway are initially expected to exhibit mass ratios of $q \sim \mathcal{O}(0.1)$ and separations of $\sim 10$ pc. The secondary black hole, initially embedded in a dense massive gas cloud ($n_{\rm H} \gtrsim 10^4$ cm$^{-3}$, $M_{\rm cloud} \sim \mathcal{O}(10^5)\ M_\odot$) will experience enhanced accretion greatly exceeding the Eddington limit (for a $10^5\ M_\odot$ BH seed, the accretion rate attains $\eta \sim 100$ within this dense gas cloud). At this stage, the internal accretion feedback from the secondary BH is not able to stop the accretion flow (see e.g., D. Toyouchi et al. 2021), and the BH can grow rapidly at a very short time scale before the external feedback from the PBH destroys the cloud, which quickly drives the mass ratio closer to unity. This also implies that the secondary BH will become a more luminous source than the primary PBH during this phase, as the PBH only accretes at $\eta \sim 0.1 - 0.01$. If dynamical friction between the newly formed DCBH and gas effectively facilitates orbital decay, these systems may evolve into tightly bound binaries with separations $\lesssim 1$ pc on relatively short timescales (see e.g., D. Fiacconi et al. 2013).

After the mass of the secondary BH catches up with the PBH and the binary becomes tightly bound, this scenario could offer a compelling explanation for enigmatic high-redshift sources, such as the LRDs (e.g., J. Matthee et al. 2024). The characteristic V-shaped spectra of these objects could arise from dual thermal

emissions—hotter mini-disks around each SMBH and a colder circumbinary disk—according to predictions from binary accretion models (e.g., K. Inayoshi et al. 2025).

In addition, our findings have strong implications for gravitational wave astrophysics. Once in the GW-driven regime with a separation of $\sim 10^{-2} - 10^{-3}$ pc, PBH-DCBH binaries become prime targets for space-based interferometers such as LISA and TianQin, which are sensitive to SMBH coalescence within the $10^3$–$10^6$ $M_\odot$ range at millihertz frequencies (e.g., J. Luo et al. 2016; P. Amaro-Seoane et al. 2017; E.-K. Li et al. 2025). The extended inspiral phases of these binaries produce long-wavelength GW signals (e.g., K. Inayoshi et al. 2018; M. Sasaki et al. 2018), and may also contribute to the stochastic gravitational wave background detectable by PTAs, including NANOGrav, EPTA, and CPTA (e.g., G. Agazie et al. 2023; D. J. Reardon et al. 2023; EPTA Collaboration et al. 2023).

## 5. SUMMARY AND CONCLUSIONS

In this study, we have presented a novel pathway for the formation of SMBH binaries through the direct-collapse mechanism induced by a primary PBH. This PBH-induced DCBH formation channel provides a natural *in situ* mechanism for the emergence of SMBH binaries in the early Universe.

The interplay between PBH gravitational seeding, accretion-driven thermal feedback, and baryon–dark matter relative streaming motions creates favorable conditions for the accumulation and collapse of massive pristine gas clouds, as was already suggested in previous work (B. Liu et al. 2022; B. Liu & V. Bromm 2023; S. Zhang et al. 2025). Our hydrodynamical simulations demonstrate that LW radiation, locally generated by PBH accretion, significantly alters the thermal and chemical evolution of the nearby gas, suppressing molecular hydrogen cooling and shifting the dominant cooling channel to atomic hydrogen. When combined with sufficiently high initial streaming velocities ($v_{b\chi} \gtrsim 0.8\sigma_{b\chi}$), we identify a critical regime that enables the formation of gravitationally unstable, atomically-cooling gas clouds in the wake of the PBH trajectory.

During the collapse phase, our simulations show that gas inflow rates consistently exceed the threshold for DCBH formation, with $\dot{M}_{\rm infall} \gtrsim 0.01 - 0.1\ M_\odot\,{\rm yr}^{-1}$. This leads to the inevitable and rapid formation of compact massive cores within the mass range of $\sim 5\times10^4 - 10^5\ M_\odot$ in $\sim 5$ Myr. The resulting SMBH binaries exhibit initial mass ratios of $q \sim \mathcal{O}(0.1)$ and separations of $\sim 10$ pc, naturally evolving into gravitationally bound systems.

These PBH-DCBH binary systems are also promising sources of gravitational waves, potentially detectable with next-generation observatories such as LISA and TianQin (e.g., J. Luo et al. 2016; P. Amaro-Seoane et al. 2017; E.-K. Li et al. 2025). Furthermore, they may serve as plausible progenitors of binary SMBHs that are invoked to explain the distinct spectral features observed in select high-$z$ JWST/ALMA targets, such as a subset of LRDs (e.g., I. Labbe et al. 2025). Future work should explore a broader range of PBH masses and spatial distributions, investigating the long-term dynamical evolution of PBH-DCBH binaries in realistic cosmological environments, and consider the multi-frequency radiative transfer around these sources to derive their detailed observational signatures. Altogether, these findings establish a fundamental connection between early-Universe black hole physics, multi-messenger astrophysics, and the broader study of dark matter.

## ACKNOWLEDGMENTS

BL gratefully acknowledges the funding of the Royal Society University Research Fellowship and the Deutsche Forschungsgemeinschaft (DFG, German Research Foundation) under Germany's Excellence Strategy EXC 2181/1 - 390900948 (the Heidelberg STRUCTURES Excellence Cluster). The authors acknowledge the Texas Advanced Computing Center (TACC) for providing HPC resources under allocation AST23026.

*Software:* astropy ( Astropy Collaboration et al. 2013, 2018), Colossus (B. Diemer 2018)

## REFERENCES

Abel, T., Anninos, P., Zhang, Y., & Norman, M. L. 1997, NewA, 2, 181, doi: 10.1016/S1384-1076(97)00010-9

Afshordi, N., McDonald, P., & Spergel, D. N. 2003, ApJL, 594, L71, doi: 10.1086/378763

Agarwal, B., Smith, B., Glover, S., Natarajan, P., & Khochfar, S. 2016, MNRAS, 459, 4209, doi: 10.1093/mnras/stw929

Agazie, G., Anumarlapudi, A., Archibald, A. M., et al. 2023, ApJL, 951, L50, doi: 10.3847/2041-8213/ace18a

Ali-Haïmoud, Y., & Kamionkowski, M. 2017, PhRvD, 95, 043534, doi: 10.1103/PhysRevD.95.043534

Amaro-Seoane, P., Audley, H., Babak, S., et al. 2017, arXiv e-prints, arXiv:1702.00786, doi: 10.48550/arXiv.1702.00786

Astropy Collaboration, Robitaille, T. P., Tollerud, E. J., et al. 2013, A&A, 558, A33, doi: 10.1051/0004-6361/201322068

Astropy Collaboration, Price-Whelan, A. M., Sipőcz, B. M., et al. 2018, AJ, 156, 123, doi: 10.3847/1538-3881/aabc4f

Becerra, F., Marinacci, F., Bromm, V., & Hernquist, L. E. 2018a, MNRAS, 480, 5029, doi: 10.1093/mnras/sty2210

Becerra, F., Marinacci, F., Inayoshi, K., Bromm, V., & Hernquist, L. E. 2018b, ApJ, 857, 138, doi: 10.3847/1538-4357/aab8f4

Begelman, M. C., Blandford, R. D., & Rees, M. J. 1980, Nature, 287, 307, doi: 10.1038/287307a0

Begelman, M. C., Volonteri, M., & Rees, M. J. 2006, MNRAS, 370, 289, doi: 10.1111/j.1365-2966.2006.10467.x

Belotsky, K. M., Dokuchaev, V. I., Eroshenko, Y. N., et al. 2019, Eur. Phys. J. C, 79, 246, doi: 10.1140/epjc/s10052-019-6741-4

Bogdán, Á., Goulding, A. D., Natarajan, P., et al. 2024, Nature Astronomy, 8, 126, doi: 10.1038/s41550-023-02111-9

Bromm, V. 2013, Reports on Progress in Physics, 76, 112901, doi: 10.1088/0034-4885/76/11/112901

Bromm, V., Coppi, P. S., & Larson, R. B. 2002, ApJ, 564, 23, doi: 10.1086/323947

Bromm, V., & Loeb, A. 2003, ApJ, 596, 34, doi: 10.1086/377529

Cappelluti, N., Hasinger, G., & Natarajan, P. 2022, ApJ, 926, 205, doi: 10.3847/1538-4357/ac332d

Carr, B., Clesse, S., García-Bellido, J., & Kühnel, F. 2021, Physics of the Dark Universe, 31, 100755, doi: 10.1016/j.dark.2020.100755

Carr, B., & Kühnel, F. 2020, Annual Review of Nuclear and Particle Science, 70, 355, doi: 10.1146/annurev-nucl-050520-125911

Carr, B., & Silk, J. 2018, MNRAS, 478, 3756, doi: 10.1093/mnras/sty1204

Carr, B. J. 1975, ApJ, 201, 1, doi: 10.1086/153853

Casanueva-Villarreal, C., Padilla, N., Tissera, P. B., Liu, B., & Bromm, V. 2025, arXiv e-prints, arXiv:2505.10706, doi: 10.48550/arXiv.2505.10706

Chon, S., & Omukai, K. 2020, MNRAS, 494, 2851, doi: 10.1093/mnras/staa863

Chon, S., & Omukai, K. 2025, MNRAS, 539, 2561, doi: 10.1093/mnras/staf598

Colazo, P. E., Stasyszyn, F., & Padilla, N. 2024, A&A, 685, L8, doi: 10.1051/0004-6361/202449565

Dayal, P., & Maiolino, R. 2025, arXiv e-prints, arXiv:2506.08116, doi: 10.48550/arXiv.2506.08116

De Luca, V., Desjacques, V., Franciolini, G., Malhotra, A., & Riotto, A. 2019, JCAP, 2019, 018, doi: 10.1088/1475-7516/2019/05/018

De Luca, V., Franciolini, G., Pani, P., & Riotto, A. 2020, JCAP, 2020, 044, doi: 10.1088/1475-7516/2020/06/044

De Rosa, A., Vignali, C., Bogdanović, T., et al. 2019, NewAR, 86, 101525, doi: 10.1016/j.newar.2020.101525

Diemer, B. 2018, ApJS, 239, 35, doi: 10.3847/1538-4365/aaee8c

Draine, B. T., & Bertoldi, F. 1996, ApJ, 468, 269, doi: 10.1086/177689

EPTA Collaboration, InPTA Collaboration, Antoniadis, J., et al. 2023, A&A, 678, A50, doi: 10.1051/0004-6361/202346844

Escrivà, A. 2022, Universe, 8, 66, doi: 10.3390/universe8020066

Fiacconi, D., Mayer, L., Roškar, R., & Colpi, M. 2013, ApJL, 777, L14, doi: 10.1088/2041-8205/777/1/L14

Galli, D., & Palla, F. 2013, ARA&A, 51, 163, doi: 10.1146/annurev-astro-082812-141029

Goulding, A. D., Greene, J. E., Setton, D. J., et al. 2023, ApJL, 955, L24, doi: 10.3847/2041-8213/acf7c5

Greene, J. E., Labbe, I., Goulding, A. D., et al. 2024, ApJ, 964, 39, doi: 10.3847/1538-4357/ad1e5f

Haemmerlé, L. 2021, A&A, 647, A83, doi: 10.1051/0004-6361/202039686

Haemmerlé, L., Woods, T. E., Klessen, R. S., Heger, A., & Whalen, D. J. 2018, MNRAS, 474, 2757, doi: 10.1093/mnras/stx2919

Hahn, O., & Abel, T. 2011, MNRAS, 415, 2101, doi: 10.1111/j.1365-2966.2011.18820.x

Hawking, S. 1971, Monthly Notices of the Royal Astronomical Society, 152, 75

Herrington, N. P., Whalen, D. J., & Woods, T. E. 2023, MNRAS, 521, 463, doi: 10.1093/mnras/stad572

Hirano, S., Yoshida, N., Sakurai, Y., & Fujii, M. S. 2018, ApJ, 855, 17, doi: 10.3847/1538-4357/aaaaba

Hirano, S., Zhu, N., Yoshida, N., Spergel, D., & Yorke, H. W. 2015, ApJ, 814, 18, doi: 10.1088/0004-637X/814/1/18

Hobbs, G., & Dai, S. 2017, National Science Review, 4, 707, doi: 10.1093/nsr/nwx126

Hopkins, P. F. 2015, MNRAS, 450, 53, doi: 10.1093/mnras/stv195

Hosokawa, T., Yorke, H. W., Inayoshi, K., Omukai, K., & Yoshida, N. 2013, ApJ, 778, 178, doi: 10.1088/0004-637X/778/2/178

Huang, H.-L., Jiang, J.-Q., & Piao, Y.-S. 2024, PhRvD, 110, 103540, doi: 10.1103/PhysRevD.110.103540

Inayoshi, K., Ichikawa, K., & Haiman, Z. 2018, ApJL, 863, L36, doi: 10.3847/2041-8213/aad8ad

Inayoshi, K., Omukai, K., & Tasker, E. 2014, MNRAS, 445, L109, doi: 10.1093/mnrasl/slu151

Inayoshi, K., Shangguan, J., Chen, X., Ho, L. C., & Haiman, Z. 2025, arXiv e-prints, arXiv:2505.05322, doi: 10.48550/arXiv.2505.05322

Inayoshi, K., Visbal, E., & Haiman, Z. 2020, ARA&A, 58, 27, doi: 10.1146/annurev-astro-120419-014455

Inman, D., & Ali-Haïmoud, Y. 2019, PhRvD, 100, 083528, doi: 10.1103/PhysRevD.100.083528

Ito, M., & Omukai, K. 2024, PASJ, 76, 850, doi: 10.1093/pasj/psae054

Jiao, H., Brandenberger, R., & Refregier, A. 2024, PhRvD, 109, 123524, doi: 10.1103/PhysRevD.109.123524

Johnson, J. L., & Bromm, V. 2006, MNRAS, 366, 247, doi: 10.1111/j.1365-2966.2005.09846.x

Kashlinsky, A. 2021, PhRvL, 126, 011101, doi: 10.1103/PhysRevLett.126.011101

Klessen, R. S., & Glover, S. C. O. 2023, ARA&A, 61, 65, doi: 10.1146/annurev-astro-071221-053453

Kocevski, D. D., Finkelstein, S. L., Barro, G., et al. 2024, arXiv e-prints, arXiv:2404.03576, doi: 10.48550/arXiv.2404.03576

Kokorev, V., Caputi, K. I., Greene, J. E., et al. 2024, ApJ, 968, 38, doi: 10.3847/1538-4357/ad4265

Kovács, O. E., Bogdán, Á., Natarajan, P., et al. 2024, ApJL, 965, L21, doi: 10.3847/2041-8213/ad391f

Labbé, I., van Dokkum, P., Nelson, E., et al. 2023, Nature, 616, 266, doi: 10.1038/s41586-023-05786-2

Labbe, I., Greene, J. E., Bezanson, R., et al. 2025, ApJ, 978, 92, doi: 10.3847/1538-4357/ad3551

Larson, R. L., Finkelstein, S. L., Kocevski, D. D., et al. 2023, ApJL, 953, L29, doi: 10.3847/2041-8213/ace619

Latif, M. A., Khochfar, S., & Whalen, D. 2020, ApJL, 892, L4, doi: 10.3847/2041-8213/ab7c61

Latif, M. A., Whalen, D. J., Khochfar, S., Herrington, N. P., & Woods, T. E. 2022, Nature, 607, 48, doi: 10.1038/s41586-022-04813-y

Leung, G. C. K., Finkelstein, S. L., Pérez-González, P. G., et al. 2024, arXiv e-prints, arXiv:2411.12005. https://arxiv.org/abs/2411.12005

Li, E.-K., Liu, S., Torres-Orjuela, A., et al. 2025, Reports on Progress in Physics, 88, 056901, doi: 10.1088/1361-6633/adc9be

Liu, B., & Bromm, V. 2018, MNRAS, 476, 1826, doi: 10.1093/mnras/sty350

Liu, B., & Bromm, V. 2022, ApJL, 937, L30, doi: 10.3847/2041-8213/ac927f

Liu, B., & Bromm, V. 2023, arXiv e-prints, arXiv:2312.04085, doi: 10.48550/arXiv.2312.04085

Liu, B., Gurian, J., Inayoshi, K., et al. 2024, MNRAS, 534, 290, doi: 10.1093/mnras/stae2066

Liu, B., Zhang, S., & Bromm, V. 2022, MNRAS, 514, 2376, doi: 10.1093/mnras/stac1472

Lodato, G., & Natarajan, P. 2006, MNRAS, 371, 1813, doi: 10.1111/j.1365-2966.2006.10801.x

Loeb, A., & Rasio, F. A. 1994, ApJ, 432, 52, doi: 10.1086/174548

Lu, P., Takhistov, V., Gelmini, G. B., et al. 2021, ApJL, 908, L23, doi: 10.3847/2041-8213/abdcb6

Lu, Y., Picker, Z. S. C., & Kusenko, A. 2024, PhRvD, 109, 123016, doi: 10.1103/PhysRevD.109.123016

Luo, J., Chen, L.-S., Duan, H.-Z., et al. 2016, Classical and Quantum Gravity, 33, 035010, doi: 10.1088/0264-9381/33/3/035010

Ma, L., Hopkins, P. F., Ma, X., et al. 2021, MNRAS, 508, 1973, doi: 10.1093/mnras/stab2713

Mack, K. J., Ostriker, J. P., & Ricotti, M. 2007, ApJ, 665, 1277, doi: 10.1086/518998

Maiolino, R., Scholtz, J., Curtis-Lake, E., et al. 2024, A&A, 691, A145, doi: 10.1051/0004-6361/202347640

Maiolino, R., Uebler, H., D'Eugenio, F., et al. 2025, arXiv e-prints, arXiv:2505.22567, doi: 10.48550/arXiv.2505.22567

Matsuoka, Y., Izumi, T., Onoue, M., et al. 2024, ApJL, 965, L4, doi: 10.3847/2041-8213/ad35c7

Matthee, J., Naidu, R. P., Brammer, G., et al. 2024, ApJ, 963, 129, doi: 10.3847/1538-4357/ad2345

Meszaros, P. 1975, A&A, 38, 5

Milosavljević, M., & Merritt, D. 2003a, in American Institute of Physics Conference Series, Vol. 686, The Astrophysics of Gravitational Wave Sources, ed. J. M. Centrella (AIP), 201–210, doi: 10.1063/1.1629432

Milosavljević, M., & Merritt, D. 2003b, ApJ, 596, 860, doi: 10.1086/378086

Mirbabayi, M., Gruzinov, A., & Noreña, J. 2020, JCAP, 2020, 017, doi: 10.1088/1475-7516/2020/03/017

Nagele, C., Umeda, H., Takahashi, K., Yoshida, T., & Sumiyoshi, K. 2022, MNRAS, 517, 1584, doi: 10.1093/mnras/stac2495

Napolitano, L., Castellano, M., Pentericci, L., et al. 2024, arXiv e-prints, arXiv:2410.18763, doi: 10.48550/arXiv.2410.18763

Natarajan, P., Pacucci, F., Ricarte, A., et al. 2024, ApJL, 960, L1, doi: 10.3847/2041-8213/ad0e76
Negri, A., & Volonteri, M. 2017, MNRAS, 467, 3475, doi: 10.1093/mnras/stx362
Oh, S. P., & Haiman, Z. 2002, ApJ, 569, 558, doi: 10.1086/339393
Planck Collaboration, Aghanim, N., Akrami, Y., et al. 2020, A&A, 641, A6, doi: 10.1051/0004-6361/201833910
Popović, L. Č. 2012, NewAR, 56, 74, doi: 10.1016/j.newar.2011.11.001
Prole, L. R., Regan, J. A., Mehta, D., Coles, P., & Dayal, P. 2025, arXiv e-prints, arXiv:2506.11233, doi: 10.48550/arXiv.2506.11233
Qin, W., Kumar, S., Natarajan, P., & Weiner, N. 2025, arXiv e-prints, arXiv:2506.13858, doi: 10.48550/arXiv.2506.13858
Reardon, D. J., Zic, A., Shannon, R. M., et al. 2023, ApJL, 951, L6, doi: 10.3847/2041-8213/acdd02
Reisswig, C., Ott, C. D., Abdikamalov, E., et al. 2013, PhRvL, 111, 151101, doi: 10.1103/PhysRevLett.111.151101
Ricotti, M., Ostriker, J. P., & Mack, K. J. 2008, ApJ, 680, 829, doi: 10.1086/587831
Roedig, C., Krolik, J. H., & Miller, M. C. 2014, ApJ, 785, 115, doi: 10.1088/0004-637X/785/2/115
Romano, J. D., & Cornish, N. J. 2017, Living Reviews in Relativity, 20, 2, doi: 10.1007/s41114-017-0004-1
Sasaki, M., Suyama, T., Tanaka, T., & Yokoyama, S. 2018, Classical and Quantum Gravity, 35, 063001, doi: 10.1088/1361-6382/aaa7b4
Schauer, A. T. P., Boylan-Kolchin, M., Colston, K., et al. 2023, ApJ, 950, 20, doi: 10.3847/1538-4357/accc2c
Schauer, A. T. P., Glover, S. C. O., Klessen, R. S., & Ceverino, D. 2019, MNRAS, 484, 3510, doi: 10.1093/mnras/stz013
Schauer, A. T. P., Regan, J., Glover, S. C. O., & Klessen, R. S. 2017, MNRAS, 471, 4878, doi: 10.1093/mnras/stx1915
Sesana, A. 2013, MNRAS, 433, L1, doi: 10.1093/mnrasl/slt034
Shibata, M., Fujibayashi, S., Jockel, C., & Kawaguchi, K. 2025, ApJ, 978, 58, doi: 10.3847/1538-4357/ad93a4
Shibata, M., & Shapiro, S. L. 2002, ApJL, 572, L39, doi: 10.1086/341516
Springel, V. 2005, MNRAS, 364, 1105, doi: 10.1111/j.1365-2966.2005.09655.x
Stacy, A., Bromm, V., & Loeb, A. 2011, ApJL, 730, L1, doi: 10.1088/2041-8205/730/1/L1
Stahler, S. W., Shu, F. H., & Taam, R. E. 1980, ApJ, 241, 637, doi: 10.1086/158377
Suazo, M., Prieto, J., Escala, A., & Schleicher, D. R. G. 2019, ApJ, 885, 127, doi: 10.3847/1538-4357/ab45eb
Sugimura, K., Omukai, K., & Inoue, A. K. 2014, MNRAS, 445, 544, doi: 10.1093/mnras/stu1778
Takhistov, V., Lu, P., Gelmini, G. B., et al. 2022, JCAP, 2022, 017, doi: 10.1088/1475-7516/2022/03/017
Taylor, A. J., Finkelstein, S. L., Kocevski, D. D., et al. 2024, arXiv e-prints, arXiv:2409.06772, doi: 10.48550/arXiv.2409.06772
Toyouchi, D., Inayoshi, K., Hosokawa, T., & Kuiper, R. 2021, ApJ, 907, 74, doi: 10.3847/1538-4357/abcfc2
Toyouchi, D., Inayoshi, K., Li, W., Haiman, Z., & Kuiper, R. 2023, MNRAS, 518, 1601, doi: 10.1093/mnras/stac3191
Tremmel, M., Karcher, M., Governato, F., et al. 2017, MNRAS, 470, 1121
Trinca, A., Schneider, R., Valiante, R., et al. 2022, MNRAS, 511, 616, doi: 10.1093/mnras/stac062
Übler, H., Maiolino, R., Pérez-González, P. G., et al. 2024, MNRAS, 531, 355, doi: 10.1093/mnras/stae943
Valtaoja, L., Valtonen, M. J., & Byrd, G. G. 1989, ApJ, 343, 47, doi: 10.1086/167683
Westernacher-Schneider, J. R., Zrake, J., MacFadyen, A., & Haiman, Z. 2022, PhRvD, 106, 103010, doi: 10.1103/PhysRevD.106.103010
White, S. D. M., & Frenk, C. S. 1991, ApJ, 379, 52, doi: 10.1086/170483
White, S. D. M., & Rees, M. J. 1978, MNRAS, 183, 341, doi: 10.1093/mnras/183.3.341
Wolcott-Green, J., Haiman, Z., & Bryan, G. L. 2011, MNRAS, 418, 838, doi: 10.1111/j.1365-2966.2011.19538.x
Woods, T. E., Patrick, S., Whalen, D. J., & Heger, A. 2024, ApJ, 960, 59, doi: 10.3847/1538-4357/ad054a
Woods, T. E., Agarwal, B., Bromm, V., et al. 2019, PASA, 36, e027, doi: 10.1017/pasa.2019.14
Xu, H., Chen, S., Guo, Y., et al. 2023, Research in Astronomy and Astrophysics, 23, 075024, doi: 10.1088/1674-4527/acdfa5
Zel'dovich, Y. B. 1970, A&A, 5, 84
Zel'dovich, Y. B., & Novikov, I. D. 1967, Soviet Ast., 10, 602
Zhang, S., Bromm, V., & Liu, B. 2024a, ApJ, 975, 139, doi: 10.3847/1538-4357/ad7b0d
Zhang, S., Liu, B., & Bromm, V. 2024b, MNRAS, 528, 180, doi: 10.1093/mnras/stad3986
Zhang, S., Liu, B., Bromm, V., et al. 2025, ApJ, 987, 185, doi: 10.3847/1538-4357/adddb4
Ziparo, F., Gallerani, S., & Ferrara, A. 2024, arXiv e-prints, arXiv:2411.03448, doi: 10.48550/arXiv.2411.03448

Ziparo, F., Gallerani, S., Ferrara, A., & Vito, F. 2022, MNRAS, 517, 1086, doi: 10.1093/mnras/stac2705